RECEIVE SIGNAL PROCESSING FOR OFDM-BASED RADAR IMAGING

Jose R. Gutierrez del Arroyo, Julie Ann Jackson, Michael A. Temple

Dept. of Electrical and Computer Engineering
Air Force Institute of Technology
Wright-Patterson AFB, OH 45433

ABSTRACT

We propose a segment averaging matched-filter solution for recovering radar phase history data from orthogonal frequency division multiplex (OFDM) signals. The impact of digital communication features—guard bands, preambles, pilots, sync symbols, and cyclic prefixes—is discussed, and the derived matched-filter solution is modified accordingly. Experimental images using generic OFDM and IEEE 802.16 WiMAX signals demonstrate the success of the proposed signal processing approach for passive bistatic radar imaging.

Index Terms— radar, bistatic, OFDM, WiMAX, 802.16

1. INTRODUCTION

Synthetic aperture radar (SAR) imaging historically employs linear frequency modulated (LFM) chirp signals. Growth of modern digital communications networks has spurred interest in orthogonal frequency division multiplex (OFDM) signals for joint radar and communications applications as well as passive bistatic radar (PBR). Most PBR literature focuses on moving target detection and tracking, e.g. [1–3]. In this paper, we extend results in [4–6] for passive radar imaging using OFDM signals (though the development holds for active bistatic and monostatic radar too). We derive a radar phase history matched-filter solution that accounts for common digital communications signal features, such as guard bands, preambles, pilot tones, synchronization symbols, and cyclic prefixes. Experimental results exhibit successful radar image formation using the proposed approach.

2. DATA COLLECTION

In this work, we assume a fixed terrestrial transmitter and an airborne receiver. For OFDM time division duplex (TDD) transmission, each base station downlink (DL) burst is followed by an uplink (UL) burst from network users. We consider the DL subframes as a pulsed radar system with constant pulse repetition frequency equal to the communication frame rate. Figure 1 shows the general data collection geometry–the center of the collection path need not align with the transmitter line of sight to scene center as depicted.

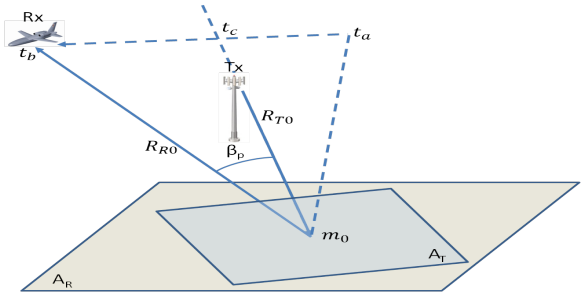

Fig. 1. General collection model–a receiver surveys area A_R which encompasses area A_T illuminated by the transmitter.

The first DL is transmitted at time t_1 and its $(l+1)$th symbol is transmitted at time $t_1 + lT_s$, where T_s is the OFDM symbol duration. Note that under a constant and stable frame rate, the same symbol position in the $(p+1)$th DL is transmitted at $t_1 + lT_s + pT_p$ where T_p is the known duration of a complete frame (DL and UL). Assuming a constant frame rate the relative transmission start time of any symbol in any DL can be determined.

On receive, the echo signal from reflection points in the scene will no longer have constant frame rate due to receiver motion. Figure 2 shows a notional data collection between times t_a and t_b. Each block represents the combined DL returns from all scatterers in the scene shifted in time by the associated path delays. Spacing between returns varies and depends on the frame rate and the bistatic range $R_{R0} + R_{T0}$, where R_{T0} is constant for a terrestrial tower transmitter. The return spacing behavior is exaggerated in Figure 2 which represents an airborne platform which is getting closer to the $\beta_p = 0$ bistatic angle. Return timing can be exploited using a transmission reference time corrected for range. Let t_r be the reference time at *any* point before the first complete DL return (any point between returns DL1 and DL2 in Figure 2). Then the same relative point for the $(p+1)$th DL return can be determined by $t_{(p+1)} = t_r + pT_p - \frac{\Delta R_{R0}}{c}$ where ΔR_{R0} is the change in receiver range between times t_r and $t_r + pT_p$.

The views expressed in this article are those of the authors and do not reflect the official policy or position of the U. S. Air Force, Dept. of Defense, or the U.S. Government. Approved for public release: 88ABW-2012-6063.

Fig. 2. Notional airborne collection with partial DL returns (1 and 5) and complete DL returns (2-4). Decreasing spacing represents decreasing platform range to scene center.

The utility of this timing approach is that the entire data collection can now be partitioned (using an envelope detector for example) into P returns, each collected from a particular bistatic aspect angle β_p. This partitioning corresponds to the typical "move-stop-move" approximation in SAR imaging, where one pulse is assumed to be transmitted/received at a fixed receiver position due to the relatively slow speed of the platform with respect to the speed of light.

Partitioning as above defines each received DL frame as a single pulse for a given receiver position, or slow-time bin. Each pulse return contains data corresponding to the scene range profile for a given receiver position. Each received DL pulse is the convolution of the transmitted waveform with the reflectivity $g(u)$ of scatterers at bistatic differential range u in the scene. The goal of SAR imaging is to recover the reflectivity for all points in the scene. To do so, each received DL pulse is processed as described in the next section.

3. SIGNAL PROCESSING

3.1. Recovering SAR Phase History

The received signal is a superposition of echoes from all scatterers and is a convolution of the scene reflectivity function (to be estimated via an image) with the transmitted signal. Deconvolution of the transmitted signal to recover the reflectivity is commonly performed via a matched filter for LFM chirp radar as derived in [7]. Work in [4,6] shows that a similar matched-filter process may be used to recover the Fourier domain representation of reflectivity, also known as the phase history, for OFDM signals. Extending the single-symbol results of [4, 6] to multiple symbols per pulse, the baseband received echo for a given DL pulse is

$$s_r(p,t)=\sum_{l=0}^{L-1}\sum_{n=-\frac{N}{2}}^{\frac{N}{2}-1} d_{l,n}e^{jn\Delta\omega(t-\tau_{l,p})}\int_{u_a}^{u_b} g(u)e^{-j(\omega_0+n\Delta\omega)\tau_{u,p}}du \tag{1}$$

where $\tau_{l,p}=\tau_0+lT_s+pT_p$ and $\tau_{u,p}$ is the bistatic differential delay of the pth pulse to a scatterer at range u. The bistatic angle for the pth pulse is β_p. Then, for $\tau_{u,p}=\frac{2}{c}u\cos(\beta_p/2)$ and $k_n=\frac{2}{c}\left(\omega_0+n\Delta\omega\right)\cos(\beta_p/2)$

$$s_r(p,t)=\sum_{l=0}^{L-1}\sum_{n=-\frac{N}{2}}^{\frac{N}{2}-1} d_{l,n}e^{jn\Delta\omega(t-\tau_{l,p})}\underbrace{\int_{u_a}^{u_b} g(u)e^{-jk_nu}du}_{G_p[k_n]} \tag{2}$$

is a Fourier series with coefficients [4, 6]

$$\sum_{l=0}^{L-1} d_{l,n}e^{-jn\Delta\omega(\tau_{l,p})}G_p[k_n]=\frac{1}{T_L}\int_0^{T_L} s_r(p,t)e^{jn\Delta\omega t}dt. \tag{3}$$

The right-hand-side of (3) is the Fourier transform $S_p(\omega_n)$ of the received signal for the pth DL. Solving for phase history $G_p[k_n]$ yields the matched-filter response

$$G_p[k_n]=\frac{\left(\sum_{l=0}^{L-1} d_{l,n}e^{-jn\Delta\omega(lT_s+pT_p)}\right)^*}{\left|\sum_{l=0}^{L-1} d_{l,n}e^{-jn\Delta\omega(lT_s+pT_p)}\right|^2}\varphi_n^{-1}S_p(\omega_n) \tag{4}$$

for $\varphi_n=e^{-jn\Delta\omega\tau_0}$ and $\left|\sum_{l=0}^{L-1} d_{l,n}e^{-jn\Delta\omega(lT_s+pT_p)}\right|\neq 0$, and where * denotes complex conjugate.

Sampling the pth pulse at an interval of T_s/N leads to the discrete matrix form of (4)

$$\boldsymbol{G}_p = \boldsymbol{D}_p^\dagger\boldsymbol{\Psi}_p^{-1}\boldsymbol{S}_p=\left[G_p[k_{-\frac{N}{2}}] \quad \cdots \quad G_p[k_{\frac{N}{2}-1}]\right]^T \tag{5}$$

$$\boldsymbol{\Psi}_p = \text{diag}\left\{\left[e^{-j\frac{N}{2}\Delta\omega\tau_0} \quad \ldots \quad e^{j\left(\frac{N}{2}-1\right)\Delta\omega\tau_0}\right]\right\} \tag{6}$$

$$\boldsymbol{D}_p^\dagger = \text{diag}\left\{\left[d^\dagger_{-\frac{N}{2}} \quad \cdots \quad d^\dagger_{\frac{N}{2}-1}\right]\right\} \tag{7}$$

$$\boldsymbol{S}_p = \left[S_p[\tfrac{c}{2}k_{-\frac{N}{2}}] \quad \cdots \quad S_p[\tfrac{c}{2}k_{\frac{N}{2}-1}]\right]^T \tag{8}$$

for $d_n^\dagger=\frac{\left(\sum_{l=0}^{L-1} d_{l,n}e^{-jn\Delta\omega(lT_s+pT_p)}\right)^*}{\left|\sum_{l=0}^{L-1} d_{l,n}e^{-jn\Delta\omega(lT_s+pT_p)}\right|^2}$ when the denominator is non-zero and $d_n^\dagger=0$ otherwise [4, 6]. Fourier inversion of $\boldsymbol{G}_p$ yields the one-dimensional range profile for the pth DL pulse. The accumulation of phase history $\boldsymbol{G}=\left[\boldsymbol{G}_1 \quad \cdots \quad \boldsymbol{G}_P\right]$ for $P>1$ pulses yields a two-dimensional image of the scene via standard SAR processing, e.g. back-projection [8] or polar reformat imaging [7].

3.2. Mitigating Inter-symbol Interference Effects

One can alternatively use *segments* of arbitrary length within a DL pulse for defining $\boldsymbol{G}$ in (4) and (5) and subsequent image processing. Averaging the computed phase history for multiple segments within a pulse provides coherent integration gain that improves image quality. We define the *segment averaging matched filter* (SAMF) version of (5) as

$$\bar{\boldsymbol{G}}_p=\frac{1}{M}\sum_{m=0}^{M-1}\boldsymbol{D}_p^\dagger\boldsymbol{\Psi}_p^{-1}\boldsymbol{S}_{p,m} \tag{9}$$

where $\boldsymbol{S}_{p,m}=\frac{1}{T_{\text{seg}}}\int_{t_m}^{t_m+T_{\text{seg}}} s_r(p,t)e^{jn\Delta\omega t}dt$ is the Fourier transform of the received signal over the mth time segment of length T_{seg}.

Figure 3 depicts the timing of OFDM symbols at the receiver. The time between near and far target echoes is T_I. An offset of T_s between the start of received echoes from adjacent symbols corresponds to the symbol transmission period.

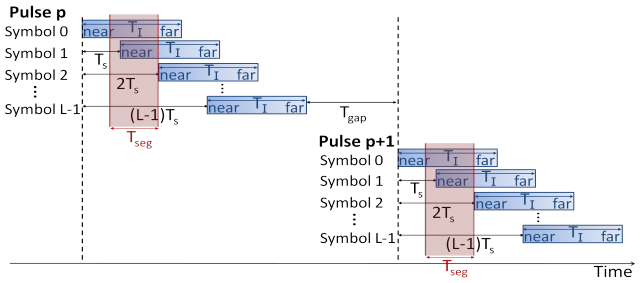

Fig. 3. Timing of OFDM symbol echoes at receiver.

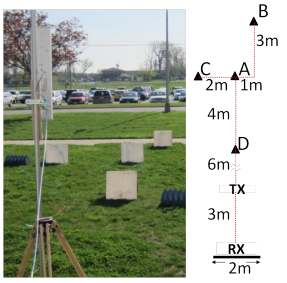

Fig. 4. Experimental bistatic setup with four plate targets.

For a sufficiently small scene size, $T_I < T_s$, and all symbol l echoes are received before symbol $l+1$ echoes begin. Typically, $T_I > T_s$, so there is overlap between OFDM symbol echoes, resulting in inter-symbol interference (ISI). For 60/40 DL/UL TDD, as implemented in all results in Section 4, there is a gap between successive DL pulses. We assume the UL is sufficiently long so after taking into account receiver motion, e.g. as in Figure 2, there remains a timing gap of T_{gap} such that successive pulse echoes do not overlap. In Figure 3, a shaded red box of width T_{seg} represents the mth segment window. Selecting T_{seg} involves a tradeoff between choosing a long enough segment to capture energy from both near and far target echoes for a given symbol and choosing a short enough segment to minimize ISI effects.

3.3. Accounting for Digital Communication Features

Real-world OFDM signals employ features such as guard bands, preambles, pilot tones, synchronization (sync) symbols, and cyclic prefixes for improved communications. These features are considered here in the context of SAR imaging.

Guard Bands. Guard bands are used in the frequency domain to reduce interference in adjacent frequency bands. OFDM subcarrier values within the guard band have amplitudes $d_{l,n} = 0$, resulting in a reduced effective bandwidth B_{eff} and consequently a coarser SAR range resolution, defined by $c/(2B_{\text{eff}}\cos(\beta/2))$, where β is the average bistatic angle over the collection. Guard bands and other instances of $d_{l,n} = 0$ (such as a null DC subcarrier) are accounted for in the pseudo-inverse form of the matched filter $\boldsymbol{D}_p^\dagger \boldsymbol{\Psi}_p^{-1}$.

Preambles, Pilot Tones, and Sync Symbols. Preambles, pilot subcarriers, and sync symbols employ predefined values of $d_{l,n}$ given by the communications standard for a given signal type. Prior knowledge of symbol timing and subcarrier utilization allows for pulse-to-pulse phase coherence for radar imaging. Furthermore, knowledge of preambles, pilots, and sync symbols allows for generation of noiseless reference signals for improved signal correlation. In this paper, we do not exploit the preambles, pilot tones, or syncs exclusively, as we have assumed the receiver has access to the entire (noiseless) transmission data $d_{l,n}$, either via cooperation of the transmitter or via processing the direct path signal. An example of using only preambles as a reference is given in Figure 6.

Cyclic Prefix. Cyclic prefixes (CP) are copies of the end of a time-domain symbol that are appended to the beginning of the symbol transmission. The CP length is generally fixed and known from the communications standard. CP replication may result in multiple correlation peaks, yielding false target detections; the processing segment length T_{seg} should be greater than the CP time to mitigate false detections. Also, the matched-filter reference signal $\boldsymbol{D}_p^\dagger$ requires modification to include CP effects. An inverse Fourier transform of the reference $d_{l,n}$ sequence, CP extension, and Fourier transform back to frequency domain provides the proper reference to build $\boldsymbol{D}_p^\dagger$ to account for the CP. Omission of the CP in the reference signal results in segment averaging of pulses with varying range shifts, resulting in a corrupted image.

4. EXPERIMENTAL RESULTS

We demonstrate PBR SAR imaging using the matched filter processes derived in Section 3. We employ the laboratory radar system described in [5] that includes an arbitrary waveform generator and digital oscilloscope linked via a local area network. The target scene and bistatic transmit/receive configuration is depicted in Figure 4.

Figure 5 shows image results for the scene in Figure 4 for a generic 60/40 TDD OFDM signal with bandwidth 344MHz, center frequency 2.3GHz, and $T_s = 0.744\mu$s. The near-to-far plate target separation results in $T_I = 0.047\mu\text{s} < T_s$, but the physical scene is actually larger than the plate-target area, so $T_I > T_s$ in practice. Given low transmit power, we can assume reflectors beyond the farthest plate have relatively low-amplitude returns resulting in very little ISI. Then, the ideal matched filter for the lth $T_{\text{seg}} = T_s$ seconds of the received signal corresponds to the lth transmitted symbol.

The images in Figure 5 compare processing for short and long segment lengths, without and with segment averaging. Since segment processing is within a pulse and not across pulses, only the image down-range dimension is affected by choice of T_{seg} and averaging. Processing a single segment of

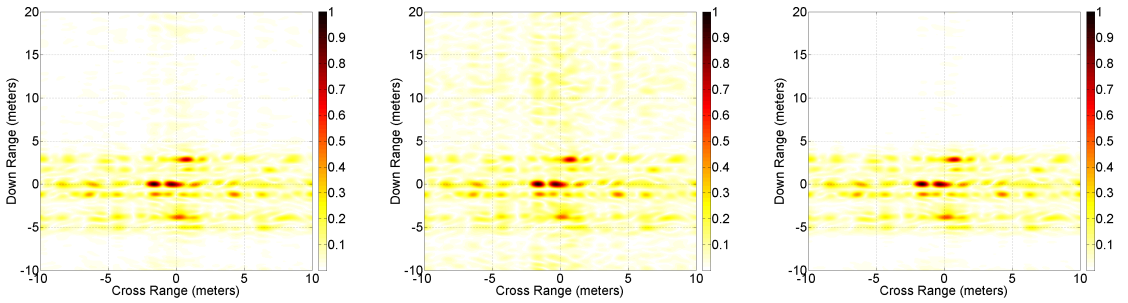

(a) First segment, $T_{\text{seg}} = T_s$ (b) Full record, $T_{\text{seg}} \approx 5.4T_s$ (c) Average over 5 segments of $T_{\text{seg}} = T_s$

Fig. 5. Experimental images for OFDM radar processed with (a) short segment (b) long segment and (c) segment averaging.

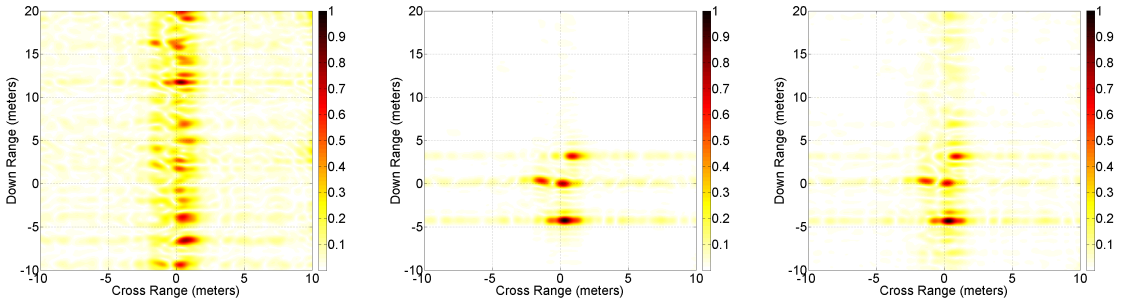

(a) SAMF without CP correction (b) SAMF with CP correction (c) Preambles only, with CP correction

Fig. 6. Experimental images for OFDM-WiMAX signal processed by (a-b) averaging over 12 segments of $T_{\text{seg}} = T_s$ and (c) a single segment of $T_{\text{seg}} = 2T_s$ including the preamble echoes only.

length $T_{\text{seg}} \approx 5.4T_s$ (full recorded return due to scope memory limitations) results in increased ISI, compared to a single segment of length $T_{\text{seg}} = T_s$; ISI effects include increased image noise as is evident, for example, in the far down-range regions of Figure 5(b). Averaging over non-overlapping segments of length T_s provides a coherent integration gain, as expected, resulting in a signal-to-noise improvement in the down-range dimension.

Figure 6 demonstrates the proposed SAMF processing approach for an IEEE 802.16 WiMAX OFDM signal [9] with center frequency 2.3GHz and bandwidth 269MHz[1]. The WiMAX signal includes guard band, preamble, pilot, and CP features discussed in Section 3.3. Figure 6 demonstrates that: 1) omission of the cyclic prefix in the reference signal results in a corrupted image due to averaging multiple pulses with different total CP time (range) shifts, and 2) successful image formation is possible over limited area using just the preamble echoes in cases where the receiver does not have access to the full transmitted data subframe.

[1]We have scaled the WiMAX signal bandwidth beyond the maximum standard definition of 20MHz to achieve reasonable range resolution for our limited experimental scene extent and low signal power. Results are a size-scaled version of achievable images with real-world WiMAX.

5. CONCLUSION

We have demonstrated successful PBR image formation using OFDM signals of opportunity. The proposed segment averaging matched filter approach reduces ISI effects and improves image quality. Inclusion of cyclic prefix, preamble, and other digital communication signal features has been accounted for and may be exploited in future work.

6. RELATION TO PRIOR WORK

Previous work has considered OFDM signals for moving target indication (MTI) [1–3]. The segment matched-filter result derived herein for SAR phase history recovery is consistent with the MTI range-doppler processing of [3]. The pseudo-inverse form of the SAMF accounts for guard bands and other null subcarriers not accounted for by [10]. The example image results extend range profile results of [5, 6, 11], and exhibit feasible application to real-world WiMAX signals, whose radar ambiguity properties are analyzed in [12–14]. Finally, the showcased images improve results in [6] which did not use segment averaging.

7. REFERENCES

[1] P. Falcone, F. Colone, C. Bongioanni, and P. Lombardo, "Experimental results for OFDM WiFi-based passive bistatic radar," in *IEEE Radar Conference*, 2010, pp. 516–521.

[2] P. Falcone, F. Colone, P. Lombardo, and T. Bucciarelli, "Range sidelobes reduction filters for wifi-based passive bistatic radar," in *European Radar Conference*, 2009, pp. 133–136, ID: 24.

[3] C. R. Berger, B. Demissie, J. Heckenbach, P. Willett, and S. Zhou, "Signal processing for passive radar using OFDM waveforms," *IEEE Journal of Selected Topics in Signal Processing*, vol. 4, no. 1, pp. 226–238, Feb. 2010.

[4] J. Gutierrez del Arroyo and J. A. Jackson, "SAR imaging using WiMAX OFDM PHY," in *IEEE Radar Conference*, 2011, pp. 129–134.

[5] J. Gutierrez del Arroyo and J. A. Jackson, "Range profiles from an experimental OFDM passive radar," in *International Waveform Diversity and Design Conference*, 2012.

[6] J. Gutierrez del Arroyo and J. A. Jackson, "WiMAX OFDM for active and passive SAR ground imaging," *IEEE Transactions on Aerospace and Electronic Systems*, Accepted for publication, June 2012.

[7] C. V. Jakowatz, D. E. Wahl, P. H. Eichel, D. C. Ghiglia, and P. A. Thompson, *Spotlight-mode synthetic aperture radar : a signal processing approach*, Kluwer Academic Publishers, Boston, 1996.

[8] D. C. Munson Jr., J. D. O'Brien, and W. K. Jenkins, "A tomographic formulation of spotlight-mode synthetic aperture radar," *Proceedings of the IEEE*, vol. 71, no. 8, pp. 917–925, 1983.

[9] LAN/MAN Standards Committee, "IEEE standard for local and metropolitan area networks. part 16: Air interface for fixed broadband wireless access systems," 2002.

[10] C. Sturm, E. Pancera, T. Zwick, and W. Wiesbeck, "A novel approach to OFDM radar processing," in *Radar Conference, 2009 IEEE*, 2009, pp. 1–4.

[11] C. Sturm, T. Zwick, W. Wiesbeck, and M. Braun, "Performance verification of symbol-based OFDM radar processing," in *Radar Conference, 2010 IEEE*, 2010, pp. 60–63.

[12] J. Gutierrez del Arroyo, J. A. Jackson, and M. A. Temple, "WiMAX ambigutity function for PCL systems," in *IEEE NAECON*, 2010.

[13] F. Colone, P. Falcone, and P. Lombardo, "Ambiguity function analysis of WiMAX transmissions for passive radar," in *Radar Conference, 2010 IEEE*, 2010, pp. 689–694.

[14] Q. Wang, C. Hou, and Y. Lu, "WiMAX signal waveform analysis for passive radar application," in *International Radar Conference*, Oct. 2009, pp. 1–6.